Arabian Journal of Chemistry (2023) **16**, 104600

King Saud University

Arabian Journal of Chemistry

www.ksu.edu.sa
www.sciencedirect.com

ORIGINAL ARTICLE

Reconstituted LH2 in multilayer membranes induced by poly-L-lysine: Structure of supramolecular and electronic states

Xiao-Lin Liu, Yuan-Yuan Hu, Kang Li, Ming-Qing Chen, Peng Wang *

Department of Chemistry, Renmin University of China, Beijing 100872, People's Republic of China

Received 23 June 2022; accepted 13 January 2023
Available online 20 January 2023

KEYWORDS

Multi-layer structure of membrane;
Light-harvesting complex 2;
Structural splitting of B850 exciton;
Photoprotection

Abstract To explore the effect of cell membrane stacking on the function of light-harvesting complex 2 (LH2) in purple nonsulfur photosynthetic bacteria, LH2 from *Rhodobacter sphaeroides* 2.4.1 (*R. sph* 2.4.1) was reconstituted into lipid bilayer vesicles (LH2@liposome) and further formed multi-layer structure by electrostatic interaction with poly-L-lysine (LH2@liposome/PLL), which was characterized by cryo-electron microscopy (cryo-EM) and TEM. When embedded in liposomes and additionally in multi-layer liposomes, the absorption band, zero-crossing point of CD signals and fluorescence emission of LH2 B850 excitons were observed to uniformly have 1–2 nm red-shifting. Combining with the corresponding fluorescence quench and the generation of shorter-living fluorescence species, a new excitonic species generated through B850 structural splitting was proposed. By FT-Raman and triplet carotenoid dynamics, the structural mechanism was deduced and discussed. Briefly, all environmental changes, including LH2 aggregating and multi-layer membrane stacking, eventually applied forces on B850 exciton molecules mainly through the hydrogen bonding between the C3-acetyl carbonyl groups of B850 BChls and Tyr44 and 45 residues at C-terminus of α-polypeptides. The effect of multi-layer structure on LH2 could be assigned as a kind of photoprotection.

1. Introduction

The photo reaction of photosynthetic organisms was performed by a series of protein complexes embedded on photosynthetic membranes (Singharoy et al., 2019; Hohmann-Marriott et al., 2011; Blankenship, 2008). To adapt variable light conditions in natural environment, phototrophs evolved various structural mechanisms to regulate the photon energy utilization, including photon capture, excitation energy transfer, and distribution of the excitation in various photosystems (Rochaix, 2014; Dekker and Boekema, 2005; Sonani et al., 2018). Among these mechanisms, to dynamically control the supramolecular structure of photosynthetic membrane is one of the key methods.

* Corresponding author.
E-mail address: wpeng_chem@ruc.edu.cn (P. Wang).
Peer review under responsibility of King Saud University.

Production and hosting by Elsevier

https://doi.org/10.1016/j.arabjc.2023.104600

For higher plant, through artificially assembly, morphological characterization, and spectroscopic studies *in vitro*, researchers had clarified that the dynamical assembly and de-assembly of grana, the membrane stacking region of thylakoid membrane of chloroplast, plays key role in regulating the photosynthetic functions in many aspects (Pribil et al., 2014; Goss et al., 2007; Hepworth et al., 2021). It included enhancement of light capture, reversibly fine-tuning the energy distribution between the photosystems by state transitions, and regulating light-harvesting via controlled thermal dissipation of excess excitation energy, *i.e.* non-photochemical quenching (NQP), etc (Chow et al., 2005). The major peripheral light harvesting complexes of PSII (LHCII) and the main lipid component of thylakoid membrane (neutral glycolipids) were proved to perform key function in grana stacking (Demé et al., 2014; Albanese et al., 2020; Anderson, 1986). Recently, Li et al. (2020) proposed an environmental factor induced 'dynamical and allosteric regulation' mechanism concerning NPQ of LHC Ⅱ.

As the most ancient photosynthetic organisms on earth, purple photosynthetic bacteria were extensively studied as prototypes of algae and higher plants due to their simple composition and conserved architecture of photochemical reaction center (Cardona and Rutherford, 2019; Xiong and Bauer, 2002). As the unicellular procaryote, the photosynthetic membrane of purple bacterium is indeed the intracytoplasmic membrane (ICM) composed of various protein complexes embedded in the phospholipid bilayers. Among them, the light-harvesting peripheral complex LH2 and core complex LH1-RC perform the function of photon energy utilization (Cogdell et al., 2006; Mirkovic et al., 2017). To adapt variable photo conditions, purple bacteria regulate their photon energy absorption and EET efficiency through genetically controlling the amount and the structure of LH2 (Varga and Staehelin, 1983; Kotecha et al., 2013; Li et al., 2014; Gardiner et al. 2018), and the super-complexes structure of core complex LH1-RC (Qian et al., 2021a; Yu et al., 2018; Qian et al., 2018; Qian et al., 2013).

In addition, more researches indicate that the morphology of bacterial ICM has correlation with the functional tuning of membrane protein complexes. Through thin-section electron micrograph, the ICM of purple non-sulfur bacteria (PNSB) *Rba. sphaeroides* 2.4.1 growing under lower light condition was shown owning closely compacted vesicle arrays shape with vesicle diameter as ~ 30–50 nm, while under higher light intensity, the ICM shows the amount-decreasing vesicle array shape (Kiley and Kaplan, 1988; Adams and Hunter, 2012). The carotenoid-less mutants of *Rba. sphaeroides* and *Rsp. rubrum* preferentially generates the ICM with layer-by-layer stacking structure rather than vesicle array like (Ng et al., 2011; Lommen et al., 1978; Maudinas et al., 1973). It's worth to pointed out that carotenoids generally play three main functions in purple bacteria, *i.e.* light-harvesting assistance, photo-protection mainly by quenching the long-lived triplet *BChls*, and structural stabilization (Hashimoto et al., 2016; Fraser et al., 2001). The morphological change of ICM due to carotenoid depletion might be some compensation for its corresponding functional loss. Additionally, the similar morphology of ICM with coexisting layer-by-layer stacking structure and vesicle structure was observed too in other wild type species, *e.g. Phaeospirillum molischianum* and *Rhodopseudomonas palustris*. And the ratio of layer-by-layer stacking structure was tuned by photo intensity for growing (Varga and Staehelin, 1983; Mascle-Allemand et al., 2008; LaSarre et al., 2018; Scheuring and Sturgis, 2009). More studies displayed that photosynthetic membrane of purple bacteria facilitates the EET inter-complexes by lowering the excitation transfer times between complexes through closely packing and as a result increasing the overall quantum efficiency of the chromatophore (Hsin et al., 2010a, 2010b). Interestingly, as the counterpart of LHCII in higher plant, LH2 in purple bacteria displays the potential ability to determine the morphology of ICM *in vivo*. E.g., LH2-depletion mutant of purple bacterium *R. sph* shows tube-like ICM and the vesicle amount decreases further (Kiley et al., 1988).

In vitro, effects of lipids bilayers on the function of pigment-protein complexes were studied mainly on plane membrane (Sumino et al., 2013), liposomes (Huo et al., 2016; Dai et al., 2018; Niedzwiedzki et al., 2016; Freiberg et al., 2012; Ikemoto et al., 2013), or nanodiscs (Ogren et al.,2018). Almost no study by artificial simulation was reported on the relationship between ICM morphology of purple bacteria, especially the membrane stacking or vesicle array structures, and its regulating mechanism of photo energy utilization.

Positively charged poly-L-lysine (PLL) has the ability of assembling the liposomes with negatively charges to form multi-layer structures (Seyrig et al., 2020a, 2020b). In this research, to simulate the multi-layers structure of ICM of purple bacteria and to study their effect on the structural and photon energy utilizing mechanism of embedded pigment-protein complexes, we choose LH2 from *R. sph* 2.4.1 and the soybean lecithin to construct the multi-layered structure of liposome with incorporated LH2 through electrostatic interaction with PLL. By a series of spectroscopic and morphological characterization methods, the structural and excited state properties affected by the multi-layer structure were discussed in comparison with the LH2 in detergent micelle and in liposome. This exploration might contribute to the further artificial simulation work at this respect.

2. Methods and materials

Tris(hydroxymethyl)aminomethane (Tris) (>99 %) and diethylaminoethyl cellulose (DEAE-52) were purchased from Solarbio life science (Beijing), and inorganic salts (both A. R.) were purchased from Sinopharm chemical reagent Beijing Co., and lauryl dimethylamine oxide (LDAO, 30 %), poly-L-lysine and egg phosphatidylcholine (PC, Mw: 776) were purchased from Sigma-Aldrich.

2.1. Purification of LH2

The bacterial cultivation and protein purification processes were similar with those described in a previous report (Niedzwiedzki et al., 2016), briefly described as followings. *R. sph* 2.4.1 was cultivated in M22 + medium under light for 3 days anaerobically, and was harvested by centrifugation. The chromatophore of *R. sph* 2.4.1 was prepared by sonication and ultracentrifugation. The obtained chromatophore was resuspended and diluted in 20 mM Tris-HCl pH 8.0 to OD_{800} = 50 cm^{-1}. LDAO was added to a final concentration of 1 %; and stirred for 45 min under N_2 atmosphere, and LH2 was purified by anion-exchange column of DEAE-52.

2.2. Preparation of LH2@liposome and LH2@liposome/PLL

The preparation of LH2@liposome was the same as that previously reported (Dai et al., 2018). Briefly, phospholipids were dissolved in $CHCl_3$ to obtain a 1 mg/mL stock solution. PC solution (3 mL) was placed into a brown glass bottle, and the solvent was removed by N_2 and dried under vacuum for 4 h. Then, 2.63 mL of Tris-HCl buffer (20 mM, pH 8.0) and 0.1 mL of 30 % LDAO were added, and PC was dissolved by sonication. A 270 μL of LH2 from *R. sph* 2.4.1 (OD_{849} = 22.7 cm^{-1}, ε_{B850} = 3.23 ± 0.03 $M^{-1}cm^{-1}$ (Saga and Hirota, 2016) was added and vortexed gently for 30 s. LH2@liposome were prepared by dialyzing against detergent-free buffer in the dark at 4 ℃ for 3 times (3 h, 3 h, and 18 h) and then homogenized by ultrafiltration through a film with pore size of 220 nm for 10 times.

40 μL of 1 mg/mL PLL solution was added into 2 mL LH2@liposome suspension with lipid concentration of 0.25 mg/mL to make PLL/lipid ratio as 8 % (w/w). The resulted solutions were gently mixed and incubated in the dark at 4 ℃ for 1 h to obtain the LH2@liposome/PLL. The procedure of sample preparation was depicted in Fig. 1A.

2.3. Morphological characterization of liposome samples

The morphology of liposome samples was characterized by cryo-EM (FEI Talos F200C, Thermo Fisher Scientific, Massachusetts, USA) with a Gatan Orius CCD numeric camera and a Gatan Cryoholder (Gatan 626DH, Gatan) sample holder. The samples were slightly dropped on a glow-discharged holey carbon-coated TEM copper grid (Quantifoil R2/2, Germany). After the excess solution was removed, the grid was put into liquid ethane at − 180 ℃. The grid was then transferred into liquid nitrogen. During the experimentation, all grid temperatures were maintained by liquid nitrogen. Correspondingly, the morphology of liposome samples were also characterized by general TEM (H-7650, Hitachi, Japan).

2.4. Steady state spectroscopic measurements

UV–vis near-infrared absorption spectra were measured with a Cary-60 spectrophotometer (Agilent, USA). Each spectrum was an average of a few independent measurements at room temperature.

Fluorescence spectra were measured with FLS 980 fluorescence spectrometer (Edinburgh Instruments, UK). For fluorescence measurements, the sample concentration was adjusted to OD_{849} of LH2 as 0.04 cm^{-1}, and the excitation wavelength was 800 nm.

The particle size and surface potential of liposome samples were measured by Zetasizer Nano ZS90 (Malvern, UK). The data was an average of 3 times accumulation.

Resonance Raman spectra of the complexes (OD_{849} = 1-cm^{-1}) were recorded on the XploRA PLUS spectrometer (HORIBA, France) under laser excitation at 532 nm.

Pre-resonance Raman spectra of BChl *a* were recorded by FT-Raman spectrometer (MultiRAM; Bruker, USA), excited by a continuous-wave Nd^{3+}: YAG laser operated at 1064 nm, with a resolution of 4 cm^{-1}. The spectra were obtained by averaging 1200 scans. The sample was concentrated to OD_{849} of LH2 as 30 cm^{-1} for this measurement.

The circular dichroism (CD) spectrum was obtained by Chirascan (Applied Photophysics, UK) ranging from 190 to 1000 nm. The sample concentration was adjusted to OD_{849} = 1 cm^{-1}.

2.5. Time-Resolved spectroscopic measurement.

2.5.1. Fluorescence lifetime

Fluorescence lifetime was determined using the time-correlated single-photon counting (TCSPC) module in FLS 980 fluorescence spectrometer (Edinburgh Instruments, Edinburgh, UK). The EPL-475 picosecond pulsed diode laser (Edinburgh Instruments, Edinburgh, UK) with a pulse width of 100 to 90 ps was used for optical excitation. The instrumental response function (IRF) was measured using a 30 % silica gel aqueous solution as a scatterer and determined indeed as ~ 230 ps. The sample concentration for this measurement was adjusted to $OD_{B850\ maxima}$ = 0.04. The fluorescence lifetime was fitted by the software's program.

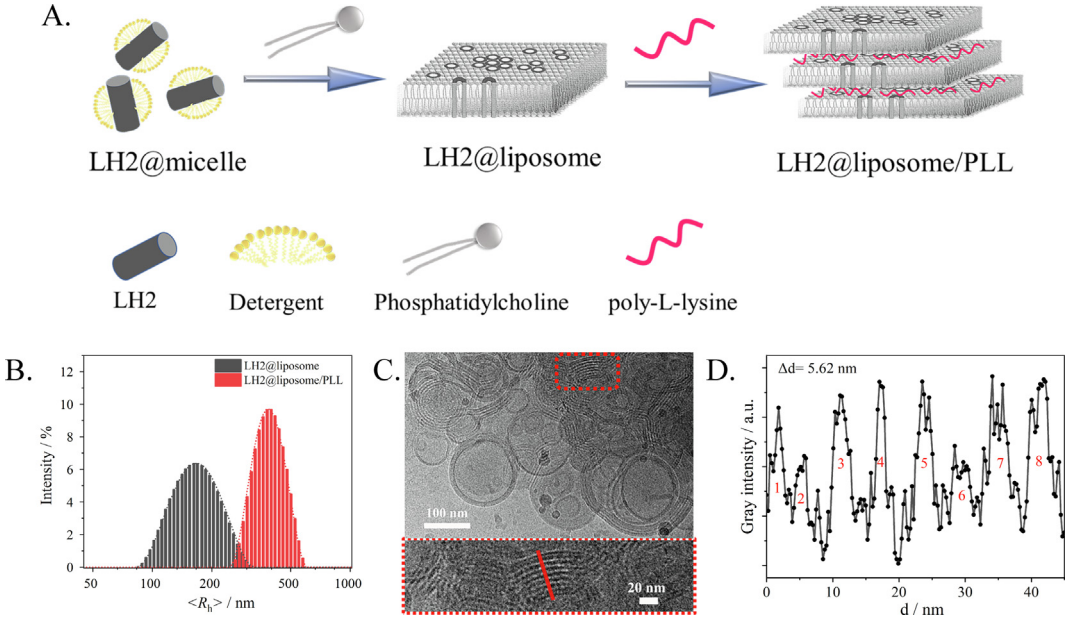

Fig. 1 (A) A cartoon of the sample preparation. (B) Particles size distribution analysis by Dynamic Light Scatter. (C) Cryo-TEM image of LH2@liposome/PLL with lipid/protein molar ratio as 2000:1. The concentration of PLL was 8% as the mass ratio of lipid. (D) Statistic estimation of the membrane thickness as Δd by gray intensity analysis on the red-line marked region of (C). Cryo-TEM data were analyzed by software ImageJ.

2.5.2. Transient absorption spectra

Transient Absorption spectra measurements were based on a home-building apparatus described detail in elsewhere (Yu et al., 2017). Briefly, the excitation pulses at 850 nm (1.4 mJ per pulse, 7 ns, 100 Hz) were supplied by an Nd: YAG laser (SpitLight DPSS EVO, InnoLas Laser Inc. Germany) while the probe light was provided by a laser-driven white light source (LDLS-EQ-1500, Energetic, USA). The temporal evolution profile of difference absorption (ΔOD) was recorded with a Si-PIN photodiode (model S3071, Hamamatsu Photonics, Japan), and output to a digital oscilloscope (LeCroy WaveSurfer 64Xs, Chestnut Ridge, USA). The full width at half maximum (FWHM) of the instrumental response function (IRF) was ~100 ns. The LH2 preparations in a quartz glass cuvette with OD_{849} = 0.5 cm^{-1}. To remove oxygen, the LH2 samples were bubbled with high purity nitrogen for 40 min before measurements. The experiments were carried out at room temperature (298 K). The least-square curve fitting programs for kinetics analyses were coded based on Matlab 5.3 (Mathworks Inc.).

3. Results and discussion

3.1. Morphology characterization of LH2@liposome and LH2@liposome/PLL

Cryo-TEM was used to characterize the morphology of membrane in liposome samples. The LH2@liposome (without PLL) was determined as monodispersed vesicles as shown as Fig. S1. The average particle size was approximately 100 nm, which is in accordance with the data measured by DLS (Fig. 1B). Comparatively, more diverse but mainly multilayered vesicular structures was observed for LH2@liposome/PLL (Fig. 1C) with increased particle size as 300–500 nm, being consistent with the DLS results (Fig. 1B). The average thickness of each layer, including membrane and the interlayer distance and shown as repeated bright and dark streak in Fig. 1B, was determined as 5.62 nm (Fig. 1D). Considering that the particle of LH2 from *R. sph* was determined as a cylinder with height of 6.6 nm (Qian et al., 2021b), at least ~ 1 nm height of the LH2 was compressed in LH2@liposome/PLL, which means that such tightly stacking multi-layer structure leaves no space between the layers. The bright and dark streaks in each layer might be due to the various density and microstructure causing different electronic diffraction effects.

In this research, the pH was buffered at 8.0, and PLL was positively charged then, since the isoelectric point of PLL was 10.5. The multi-layer structure of LH2@liposome/PLL was considered to form through electrostatic interactions between positively charged PLL and negatively charged liposomes. Such mechanism could be supported by the surface potential results of LH2@liposome (−27 mV) and LH2@liposome / PLL (+19 mV, Table S1). By general TEM (Fig. S2), on broken but extending membrane debris (due to the high vacuum under measurement) of LH2@liposome, LH2 aggregates were clearly observed with hexagonal lattice morphology (Fig. S2 A and B). Comparatively, for LH2@liposome/PLL, only tightly stacking multi-layer structure were observed (Fig. S2C), which is very similar with that observed by Cryo-EM. No LH2 particle could be observed in this sample.

3.2. UV–vis absorption and CD spectra of B850 excitons in various samples

Fig. 2A shows the normalized (at B850 maxima) UV–vis near-infrared absorption spectra of LH2 in different samples. Very similar absorption spectral patterns were observed for three samples, which suggested that the complex structure of LH2s was well maintained in liposome samples in comparison with in micelles sample. The spectra include four regions, *i.e.* Soret band of BChl *a* covering 300–400 nm, $S_0 \rightarrow S_2$ absorption of carotenoid in 450–530 nm, Q_x band of BChl *a* at 600 nm, and Q_y bands of BChl *a* at 800 nm and 850 nm. Compared with the spectrum of LH2@micelles (black line in Fig. 2A), absorption in 300–700 nm region relatively increases in LH2@liposome and LH2@liposome/PLL due to the light scattering effect originated from the enhanced particle size in liposome samples. It is worth to note that no band shift was observed in this spectral region. For BChl *a* Qy bands region, *i.e.* 750–900 nm, only the red edge of B850 band showed ~ 1 nm and 2 nm red-shift in LH2@liposome and LH2@liposome/PLL, respectively (the red and blue lines in inset of Fig. 2A), and no obvious spectral change occurred at B800 band.

Circular dichroism (CD) spectra in near-infrared region (as shown as Fig. 2B) was used to compare the chirality change of BChl *a* aggregates, *i.e.* B800 and B850 excitons, in three samples. The weaker CD signal around 800 nm (from 775 to 820 nm) was assigned to both B800 exciton and the B850 upper exciton band (Koolhaas et al., 1998; Cupellini et al., 2016). In details, the sine-signal at 795–815 nm was assigned as B800, and the negative signal at 785 nm was assigned as the upper exciton of B850. Compared with the CD signals in LH2@micelles, B800 sine shape signal in 795–815 nm region became more negative in liposome samples, LH2@liposome and LH2@liposome/PLL, while the upper exciton CD signal of B850 located at 785 nm had no change. The CD signal change in this region indicated that the chirality of B800 exciton slightly varied due to incorporation of LH2 into liposomes, although the UV–vis absorption of this region didn't have obvious change.

For the main CD signal of B850 exciton in 815–910 nm region, which was attributed to the chirality of the B850 excitonic transition, and the zero-crossing point of negative and positive peaks of B850 represented the completeness and ellipticity of the ring structure of B850 exciton (Koolhaas et al., 1998; Cupellini et al., 2016). Two characteristic variations were observed in three samples. For the first one, in liposome samples the CD signal of B850 exciton owned clearer fine structure, *e.g.* the shoulders appearing at 828 and 894 nm, than that in micelles sample, which indicated the structural splitting occurred in B850 excitons in LH2@liposome and LH2@liposome/PLL samples. The second variation is the zero-crossing point red-shifting for 1 and 2 nm, respectively, in LH2@liposome (red line in Fig. 2B) and in LH2@liposome/PLL (blue line in Fig. 2B) compared with that in LH2@micelles (black line in Fig. 2B), which is in accordance with the red-shift in the same spectral region in UV–vis absorption spectra as described above. These concomitant red-shifts implied that not only more inhomogeneity occurred in the B850 exciton coupling but also the exitonic coupling enhanced species occurred in liposome samples than in micelles sample.

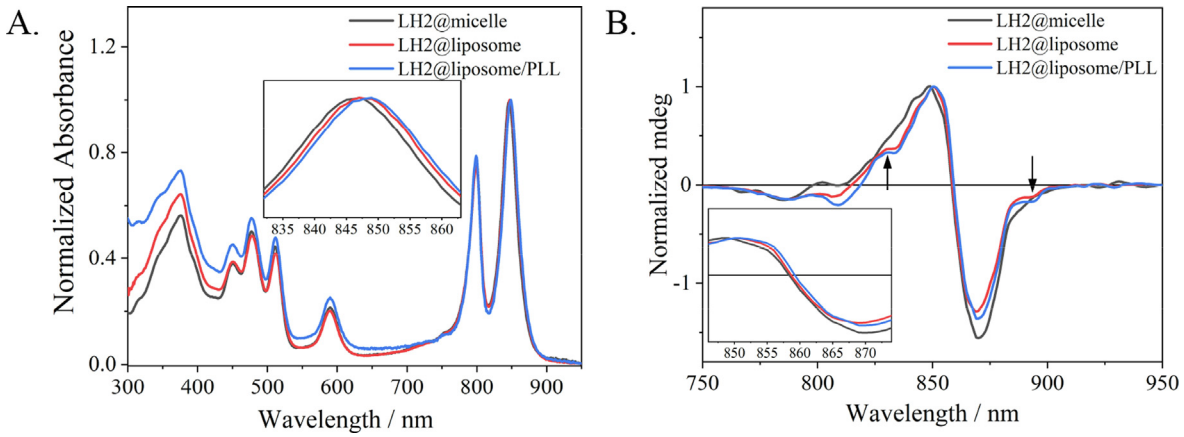

Fig. 2 (A) UV–vis absorption spectra of LH2@micelle (black), LH2@liposome (red) and LH2@liposome/PLL (blue) normalized at B850. Insert graph was B850 region of samples. (B) Circular dichroism (CD) spectra of LH2@micelle (black), LH2@liposome (red) and LH2@liposome/PLL (blue).(For interpretation of the references to colour in this figure legend, the reader is referred to the web version of this article.)

3.3. Fluorescence emission spectra and fluorescence lifetime of LH2 in different assemble systems.

Fig. 3A shows the fluorescence emission spectra of LH2 in various samples under excitation at 475 nm. When embedded into the liposomes, the fluorescence intensity of LH2@liposome (red) was ~ 27 % decrease compared with that of LH2@micelles (black), which was attributed to the aggregation of LH2 in clusters in the process of self-assembly to the phospholipid membrane and was proved by the general TEM results as shown as Fig. S2. When the liposome forms multi-layer structure induced by PLL, the fluorescence intensity of LH2@liposome/PLL decreased for ~ 80 % compared with that of LH2@micelles, which was ~ 3 times quenching effect of that of LH2@liposome. Since the same lipid/protein molar ratio was taken by the two liposome samples, the additional quenching effect besides the LH2 aggregation must originate from the multi-layer structure forming. The intrinsic structure mechanism of this quenching effect will be discussed in the following sections. Except of the fluorescence quenching effect, the fluorescence emission spectra showed 1 and 2 nm red-shift in LH2@liposome and in LH2@liposome/PLL, respectively, compared with that in LH2@micelles (see the inset of Fig. 3A). Notably, this result is in accordance with the absorption and CD signals' changes described above.

TCSPC was used to measure the fluorescence kinetics of three LH2 samples upon excitation at 475 nm and probing at 860 nm. The raw data were shown in Fig. 3B as dotted lines, and the exponential fitting results were shown as solid line (IRF as the green dashed line was determined as 230 ps). The kinetic components obtained by mono- or bi-exponentially fitting for each sample were summarized in Table 1. For LH2@micelles, only one kinetic component was obtained with the lifetime of 1.32 ns, and for LH2@liposome and LH2@liposome/PLL two kinetic species were obtained, *i.e.* a shorter lifetime as hundreds of ps and a longer one as ~ 1.40 ns. It's worth to note that the longer lifetime in liposome samples is similar with that in micelles, and the shorter lifetime with different amplitudes and different time constants in various liposome samples. In LH2@liposome,

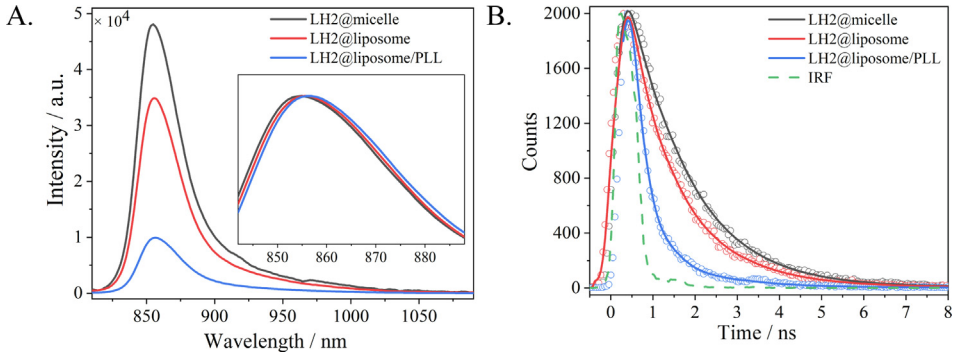

Fig. 3 (A) Fluorescent emission spectra of LH2@micelle (black), LH2@liposome (red) and LH2@liposome/PLL (blue) under excitation at 475 nm. Insert graph was the normalized fluorescence emission spectra. (B) Fluorescence kinetics probed at 860 nm for LH2@micelle (black), LH2@liposome (red) and LH2@liposome/PLL (blue), respectively, under excitation at 475 nm. IRF was shown as a green dash line.(For interpretation of the references to colour in this figure legend, the reader is referred to the web version of this article.)

Table 1 Fitting results of fluorescence kinetics probed at 860 nm in LH2@micelle, LH2@liposome and LH2@liposome/PLL.

	τ_1	Amplitude / %	τ_2	Amplitude / %	τ_{ave}
LH2@micelle	–	–	1.32	100	1.32
LH2@liposome	0.58	29.58	1.41	70.42	1.16
LH2@liposome/PLL	0.29	73.17	1.39	26.83	0.59

the shorter lifetime owns amplitude of ~ 30 % and time constant of 0.58 ns, while in LH2@liposome/PLL the shorter lifetime owns enhanced amplitude (~73 %) and decreased lifetime (0.29 ns). Such fluorescence kinetics results were well in accordance with the fluorescence intensity results as shown in Fig. 3A, which together indicated that the B850 exciton splits into two structural components when embedded into liposomes. Furthermore, the multi-layer structure formation in LH2@liposome/PLL strengthened this effect. Summarily, the new excitonic species deduced from UV–vis absorption, CD and fluorescence spectra should have the same structural origin with that observed by fluorescence kinetics measurements.

3.4. Triplet state kinetics and Resonance Raman spectra of carotenoids

Based on the high-resolution structure of LH2 from *R. sph* (Qian et al., 2021b), in each αβ-heterodimer subunit of the complex, one carotenoid (Crt) and three BChls were bound. The Crts play three main functions, *i.e.* light-harvesting assistance, photo-protection and structural stability. Concerning the photo-protection function of Crts, the long-lived triplet state of BChl *a*, arising from its excited singlet state by intersystem crossing and easily sensitizing the generation of harmful singlet oxygen, can be quenched by triplet state Crt (^{3}Crt*) nearby. Nanosecond flash photolysis was used to monitor the kinetics of ^{3}Crt* in three samples, and in other words to compare the photo-protection behaviors of Crt in three samples.

Resonance Raman spectroscopy upon excitation at 532 nm, corresponding to the $S_2 \leftarrow S_0$ absorption transition, was used to measure the conformational change of Crt as shown as Fig. 4A. The main Raman lines peaked at ~ 1517 cm^{-1} (ν_1) and ~ 1152 cm^{-1} (ν_2) were assigned as the stretching modes of conjugated C═C and C─C on skeleton, respectively. The Raman lines at ~ 1194 cm^{-1} and ~ 1001 cm^{-1} (ν_3) were attributed to the C─H bending and methyl rocking, respectively. The normalized spectra of three samples were basically overlapped with each other, which indicated that the conformation of Crt was maintained in all assemblies.

Fig. S3 A-C showed the transient absorption spectra measured at various time delays for LH2@micelle, LH2@liposome and LH2@liposome/PLL under excitation at 850 nm. Negative peaks at 450, 470 and 510 nm were attributed to the ground-state bleaching (GSB) of Crt, while the positive peaks at 520–550 nm were attributed to excited state absorption (ESA) of ^{3}Crt*, and the negative peak at 800–1000 nm was a combination of B850 fluorescence, pigments interaction band and laser interference signal. Kinetics probed at 540 and 480 nm, the representative wavelengths of ^{3}Crt* ESA and GSB, were chosen and shown in Fig. 4B for comparing the differences among three samples. All the kinetics could be perfectly fitted by mono-exponential curves. The obtained time constants were listed in Table 2 with very similar results, *i.e.* ~ 6.2 μs with < 5 % variation. The main difference concerning the kinetics for three samples was the maximal intensity of ^{3}Crt*, which were summarized in parentheses as ΔmOD. The maximal intensity of ^{3}Crt* in LH2@liposome was only 61 % of that in LH2@micelles, while that in LH2@liposome/PLL was only 28 % of that in LH2@micelles. Combining with that the conformation of Crt was almost same in all three samples, the only origin of these big differences in ^{3}Crt* yields in three samples must come from the singlet excited state yield difference of BChls. Considering the gradually increasing shorter lifetime components in LH2@liposome and LH2@liposome/PLL observed by fluorescence kinetics above, the new excitonic structure obviously quenched the singlet excited state of BChls in B850 band in liposome samples efficiently and resulted in the corresponding ^{3}Crt* yield decreases (see Table 2).

3.5. FT-Raman spectroscopy of LH2 and the possible structural mechanism

Fig. 4C exhibited the structural model of the interaction between B850 molecules and the residues of α-subunit based on the PDB ID:7PBW. It has been established that the mechanism of B850 exciton red-shifting the absorption with respect to the monomeric B800 BChls is mainly due to the close packing of the B850 BChls promoting intradimer and interdimer exciton coupling, and a further red shift is afforded by two hydrogen bonds (Qian et al., 2021b). One is between the LH2 α-Tyr45 and the C3-acetyl group on the B850 BChl-α bound to the same LH2 α polypeptide, and the other is between the neighboring residue, LH2 α-Tyr44, and the C3-acetyl group on the BChl-β bound to the LH2 β polypeptide belonging to the next αβ unit in the ring (as shown as in Fig. 4C). Qian et al. identified another hydrogen bond between α-Ser27 and the α-bound B850, which was determined without effect on the absorption maximum but only imparted stability to the LH2 complex (Qian et al., 2021b; Fowler et al., 1994; Fowler et al., 1992; Braun et al., 2003). It is worth to point out that Tyr44 and 45 located on the short helix at the end of C-terminus of α-peptide, which is perpendicular to the transmembrane helix region and is parallel with the membrane surface and stays in water–lipid interphase. The intermembrane forces were easily applied on this short helix and caused the corresponding structural changes.

Fourier transformation Raman spectra upon excitation at 1064 nm, a pre-resonance region for Qy band of BChl *a*, was used to monitor the conformational variation of BChl *a*, and the key results were shown in Fig. 4D. Please see the full spectra in Fig.S4. For each sample, six key Raman lines, denoted as R1 to R6, and, being sensitive to the BChl *a* macrocycle conformation, were used to establish the conformations of

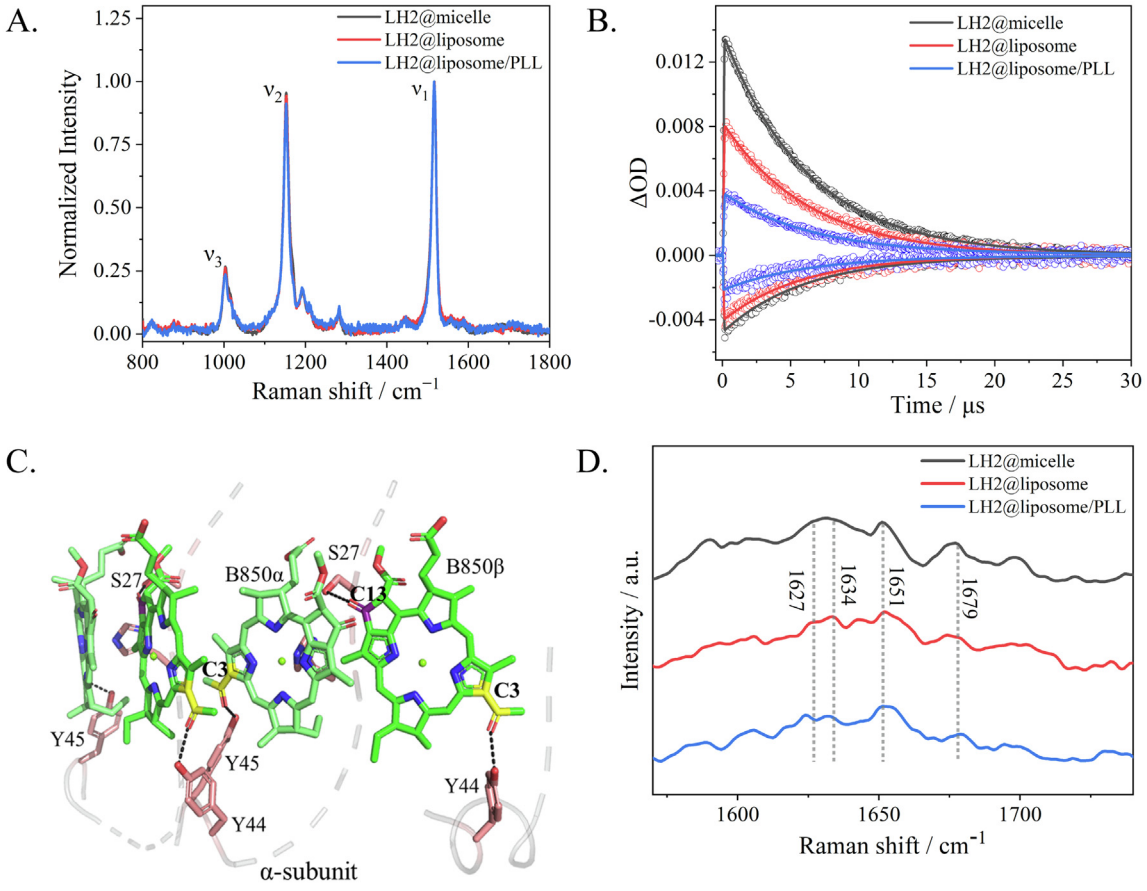

Fig. 4 (A) Resonance Raman spectra of carotenoids in three samples, *i.e.* LH2@micelle (black), LH2@liposome (red) and LH2@liposome/PLL (blue). (B) Kinetic traces of the ground state bleaching (GSB) probed at 480 nm and excited state absorption (ESA) at 530 nm of carotenoids in three samples, LH2@micelle (black), LH2@liposome (red) and LH2@liposome/PLL (blue). (C) Structural model of two adjacent B850 dimer binding sites showing hydrogen bonds between LH2 α-Tyr44, α-Tyr45, and a C3-acetyl carbonyl on each BChl. α-Ser27 is hydrogen-bonded to the $C13^1$ keto on ring V based on PDB ID: 7PBW structure. (D) Fourier transform Raman spectroscopy (FT-Raman) of LH2@micelle (black), LH2@liposome (red) and LH2@liposome/PLL (blue) range at 1570–1740 cm^{-1}.(For interpretation of the references to colour in this figure legend, the reader is referred to the web version of this article.)

Table 2 Fitting results of ^{3}Crt* GSB and ESA lifetime of LH2@micelle, LH2@liposome and LH2@liposome/PLL.

τ (ΔmOD)			
	LH2@micelle	LH2@liposome	LH2@liposome/PLL
480 nm	6.00 ± 0.01 μs (-4.6)	5.92 ± 0.03 μs (-3.8)	6.13 ± 0.05 μs (-2.1)
530 nm	6.22 ± 0.01 μs (13.3)	6.36 ± 0.01 μs (8.1)	6.49 ± 0.02 μs (3.7)

BChl *a* in LH proteins (Lapouge et al., 1999; Gall et al., 2003). The Raman shifts for 3 samples were listed in Table S2 and the assignments were based on reference (Ma et al. 2009). The key Raman lines labeled with Crt corresponding to the *v*1 (1517 cm^{-1}) and *v*2 (1152 cm^{-1}) modes of spheroidene (see above). Basically, the full spectral pattern for each sample is very similar with each other, only small signal variation was seen in three samples, which were denoted with asterisks as shown in Fig. S4. For both assemblies of LH2, the presence of methine bridge stretching at approximately 1607 cm^{-1} (R1) confirms the penta-coordination of BChl a molecule. In 1346–1444 cm^{-1} region, mainly covering the stretching mode of *v*CN on ring III and IV and the related methyl bending modes, the LH2@liposome and the LH2@liposome/PLL have Raman signals with much clearer fine structure than LH2@micelles, which indicated that upon embedded into the liposome and further forming multi-layer structure, the closely packing B850 molecules in LH2 will possess more constrained conformation especially on Ring III and IV, since these two rings of BChls were embedded deeply in the center of complexes.

Table 3 High-Frequency Carbonyl Modes of B850 in LH2.

Mode	frequency (cm^{-1})		
	LH2@micelle	LH2@liposome	LH2@liposome/PLL
B850-α C_3ν (acetyl)	1626 (sh)	1626	1623
B850-β C_3ν (acetyl)	1629	1634	1632
B850-β C_{13}ν (Keto)	1651	1651	1651
B850-α C_{13}ν (keto)	1679	1679	1679

Fig. 4C displays the higher frequency region of the FT-Raman spectra of LH2 complexes in various samples. In this region there are a cluster of bands between 1620 and 1710 cm^{-1} that are attributed to the stretching modes of the acetyl and keto- carbonyl groups (see Table 3). In the LH2 from *R. sph*, the position of each carbonyl vibrator has been established (Gall et al., 2003). The bands arising from the acetyl and keto- carbonyl stretching modes of the B800 molecules are located at 1628 and 1699 cm^{-1}. The C3-acetylcarbonyl groups of the B850 molecules contribute at ~ 1627 and ~ 1634 cm^{-1} are assigned as BChl bound to the α and β polypeptides, respectively. While the C13-keto ones are found at 1651 and 1679 cm^{-1}, respectively, assigned as B850 bound to the β and α polypeptides. The frequency of each band is sensitive to the geometry and strength of the bonding interactions that the carbonyls are involved in and may thus be used to probe the structure and intactness of the BChl binding sites (Gall et al., 2003). For LH2@micelles, the two Raman shifts attributed to C3-acetyl carbonyl groups of B850-α and B850-β move toward each other, *i.e.* the latter one down-shifting to 1629 cm^{-1} and the former one becoming a shoulder mode. While for LH2@liposome and LH2@liposome/PLL, the same pair of Raman modes are clearly resolved as 1626, 1634 cm^{-1}, and 1623, 1632 cm^{-1}, respectively. As depicted in Fig. 4C, the same α-polypeptide forms hydrogen bonding with C3-acetyl carbonyl group of B850-α and B850-β, respectively, through α-Tyr 45 and α-Tyr 44. More relaxed environments possessed by LH2@micelles than those by LH2@liposomes and LH2@liposomes/PLL might cause the former sample having more uniformed Raman modes and the latter two owning more resolved ones at these specific Raman shifts. Comparatively, the two Raman modes assigned as C13-keto carbonyl groups own almost same pair of frequencies, *i.e.* 1651 and 1679 cm^{-1}, in all three samples, only with slightly different signal patterns. Considering that the C13-keto carbonyl groups located deeply in the complexes, such small signal variation existing in three samples became reasonable.

4. Conclusions

In this research, to simulate the multi-layer structure of cytoplasmic membrane and to study their effects on the function of LH2, we firstly incorporated LH2 from *R. sph* 2.4.1 in liposomes, and then successfully prepared the multi-layer structure of LH2 in liposomes induced by poly-L-lysine (PLL) through electrostatic interactions. The multi-layer structure was characterized by Cryo-EM and TEM methods. Unlike the natural multi-layer structure of purple bacterial cytoplasmic membrane generally owning intermembrane space, the artificial multi-layer structure prepared in this research has tightly stacking and even compressed multi-layers. Based on the TEM image of LH2@liposomes, at the lipid/protein molar ratio used in this research, the LH2 aggregating on membrane were clearly observed. And by the average membrane thickness determined as ~ 5.6 nm, we estimated that ~ 1 nm height of LH2 was compressed in LH2@liposomes/PLL sample. Such membrane stacking effect must apply additional intermembrane forces on the LH2 embedded in liposomes. We couldn't clarify whether the interaction occurs between LH2s existing in different layers or not at this moment.

In comparison with LH2@micelles, the LH2 reconstituted into liposomes, *i.e.* LH2@liposome, has synchronously red-shifting (~1 nm) UV–vis absorption, zero-crossing point of CD signal and fluorescence emission bands of B850 exciton. In addition, a shorter-living fluorescence kinetics species was determined for B850 excitons. Two structural effects could be proposed to explain the above spectroscopic results. The first one is that the enhanced lateral forces from surrounding lipid molecules was applied on LH2 complex in LH2@liposomes rather than in LH2@micelles. This can be supported by the nano-disc study of LH2 (Ogren et al.,2018). In this study, the surrounding lipids was proved to cause the EET efficiency decreases between B800 and B850 intra-complexes. The second one is that the interaction between aggregated LH2s on liposome membrane generates more forces on each LH2 than that in micelles, which generally causes faster quench of excitation energy in LH2s (Sumino et al., 2013; Pflock et al., 2008). Combining all the spectroscopic results, we deduced that a new excitonic component forms in B850 excitons upon reconstituted in liposomes. In details, due to the two additional structural effects applied on LH2s in lipid bilayers, the circular B850 exciton might deform and generate structural splitting, which was evidenced by the spectral change at B850 CD signals. When the multi-layer structure forms induced by PLL, *i.e.* LH2@liposomes/PLL, more red-shifting results of the same series of spectroscopic measurements were obtained. And the fluorescence kinetics analysis gave the short-lifetime species with enhanced amplitude and shortened life constant. Such results can be explained by the 3rd structural effect in combination with the former two effects. The 3rd effect is the membrane stacking effect, which applied additional force on the B850 exciton through surrounding polypeptides, specifically the α-polypeptide. The last effect could be demonstrated by FT-Raman results. As depicted in Fig. 4C, the α-Tyr 44 and 45 located at the C-terminus of α-polypeptide can easily transfer the forces from environments to B850 excitons through the hydrogen-bonding with the C3-acetyl carbonyl group on the corresponding B850 molecules.

Summarily, either by reconstitution into the liposome or by additionally forming the multi-layer structure, all environmental effects finally were applied on B850 excitons through its hydrogen-bonding polypeptides to cause its structural splitting and to form the red-shifting and short-living new excitonic species, which eventually quenched the singlet excited state of B850 and resulted in some kind of 'photoprotection' effect. Our research paves the road to simulate more natural and dynamic supramolecular structures and study their function in regulating the EET of photosynthetic organisms.

Declaration of Competing Interest

The authors declare that they have no known competing financial interests or personal relationships that could have appeared to influence the work reported in this paper.

Acknowledgments

This work has been supported by the National Natural Science Foundation of China Nos. 22073113.

Appendix A. Supplementary data

Supplementary data to this article can be found online at https://doi.org/10.1016/j.arabjc.2023.104600.

References

Adams, P.G., Hunter, C.N., 2012. Adaptation of intracytoplasmic membranes to altered light intensity in *Rhodobacter sphaeroides*. Biochim. Biophys. Acta – Bioenerg. 1817 (9), 1616–1627. https://doi.org/10.1016/j.bbabio.2012.05.013.

Albanese, P., Tamara, S., Saracco, G., Scheltema, R.A., Pagliano, C., 2020. How paired PSII–LHCII supercomplexes mediate the stacking of plant thylakoid membranes unveiled by structural mass-spectrometry. Nat. Commun. 11 (1), 1–14. https://doi.org/10.1038/s41467-020-15184-1.

Anderson, J.M., 1986. Photoregulation of the composition, function, and structure of thylakoid membranes. Annu. Rev. Plant. Biol. 37 (1), 93–136. https://doi.org/10.1146/annurev. pp.37.060186.000521.

Blankenship, R.E., 2008. Molecular mechanisms of photosynthesis. St. Louis, Missouri.

Braun, P., Vegh, A.P., von Jan, M., Strohmann, B., Hunter, C.N., Robert, B., et al, 2003. Identification of intramembrane hydrogen bonding between 13^1 keto group of bacteriochlorophyll and serine residue α27 in the LH2 light-harvesting complex. Biochim. Biophys. Acta - Bioenerg. 1607 (1), 19–26. https://doi.org/10.1016/j.bbabio.2003.08.004.

Cardona, T., Rutherford, A.W., 2019. Evolution of photochemical reaction centres: more twists? Trends Plant Sci. 24 (11), 1008–1021. https://doi.org/10.1016/j.tplants.2019.06.016.

Chow, W.S., Kim, E.H., Horton, P., Anderson, J.M., 2005. Granal stacking of thylakoid membranes in higher plant chloroplasts: the physicochemical forces at work and the functional consequences that ensue. Photochem. Photobiol. Sci. 4 (12), 1081–1090. https://doi.org/10.1039/B507310N.

Cogdell, R.J., Gall, A., Köhler, J., 2006. The architecture and function of the light-harvesting apparatus of purple bacteria: from single molecules to in vivo membranes. Q. Rev. Biophys. 39 (3), 227–324. https://doi.org/10.1017/S0033583506004434.

Cupellini, L., Jurinovich, S., Campetella, M., Caprasecca, S., Guido, C.A., Kelly, S.M., et al, 2016. An ab initio description of the excitonic properties of LH2 and their temperature dependence. J. Phys. Chem. B. 120 (44), 11348–11359. https://doi.org/10.1021/acs.jpcb.6b06585.

Dai, L., Tan, L.M., Jiang, Y.L., Shi, Y., Wang, P., Zhang, J.P., et al, 2018. Orientation assignment of LH2 and LH1-RC complexes from *Thermochromatium tepidum* reconstituted in PC liposome and their ultrafast excitation dynamics comparison between in artificial and in natural chromatophores. Chem. Phys. Lett. 705, 78–84. https://doi.org/10.1016/j.cplett.2018.05.043.

Dekker, J.P., Boekema, E.J., 2005. Supramolecular organization of thylakoid membrane proteins in green plants. Biochim. Biophys. Acta - Bioenerg. 1706 (1–2), 12–39. https://doi.org/10.1016/j.bbabio.2004.09.009.

Demé, B., Cataye, C., Block, M.A., Maréchal, E., Jouhet, J., 2014. Contribution of galactoglycerolipids to the 3-dimensional architecture of thylakoids. FASEB J. 28 (8), 3373–3383. https://doi.org/10.1096/fj.13-247395.

Fowler, G.J.S., Visschers, R.W., Grief, G.G., Van Grondelle, R., Hunter, C.N., 1992. Genetically modified photosynthetic antenna complexes with blueshifted absorbance bands. Nature. 355 (6363), 848–850. https://doi.org/10.1038/355848a0.

Fowler, G.J.S., Sockalingum, G.D., Robert, B., Hunter, C.N., 1994. Blue shifts in bacteriochlorophyll absorbance correlate with changed hydrogen bonding patterns in light-harvesting 2 mutants of *Rhodobacter sphaeroides* with alterations at α-Tyr-44 and α-Tyr-45. Biochem. J. 299 (3), 695–700. https://doi.org/10.1042/bj2990695.

Fraser, N.J., Hashimoto, H., Cogdell, R.J., 2001. Carotenoids and bacterial photosynthesis: The story so far. Photosyn. Res. 70 (3), 249–256. https://doi.org/10.1023/A:1014715114520.

Freiberg, A., Rätsep, M., Timpmann, K., 2012. A comparative spectroscopic and kinetic study of photoexcitations in detergent-isolated and membrane-embedded LH2 light-harvesting complexes. Biochim. Biophys. Acta - Bioenerg. 1817 (8), 1471–1482. https://doi.org/10.1016/j.bbabio.2011.11.019.

Gall, A., Cogdell, R.J., Robert, B., 2003. Influence of carotenoid molecules on the structure of the bacteriochlorophyll binding site in peripheral light-harvesting proteins from *Rhodobacter sphaeroides*. Biochemistry. 42 (23), 7252–7258. https://doi.org/10.1021/bi0268293.

Gardiner, A.T., Niedzwiedzki, D.M., Cogdell, R.J., 2018. Adaptation of *Rhodopseudomonas acidophila* strain 7050 to growth at different light intensities: what are the benefits to changing the type of LH2? Faraday Discuss. 207, 471–489. https://doi.org/10.1039/C7FD00191F.

Goss, R., Oroszi, S., Wilhelm, C., 2007. The importance of grana stacking for xanthophyll cycle-dependent NPQ in the thylakoid membranes of higher plants. Physiol. Plant. 131 (3), 496–507. https://doi.org/10.1111/j.1399-3054.2007.00964.x.

Hashimoto, H., Uragami, C., Cogdell, R.J., 2016. Carotenoids and photosynthesis. In: Stange, C. (Ed.), Carotenoids in Nature. Springer, Cham, pp. 111–139.

Hepworth, C., Wood, W.H., Emrich-Mills, T.Z., Proctor, M.S., Casson, S., Johnson, M.P., 2021. Dynamic thylakoid stacking and state transitions work synergistically to avoid acceptor-side limitation of photosystem I. Nat. Plants. 7 (1), 87–98. https://doi.org/10.1038/s41477-020-00828-3.

Hohmann-Marriott, M.F., Blankenship, R.E., 2011. Evolution of photosynthesis. Annu. Rev. Plant. Biol. 62 (1), 515–548. https://doi.org/10.1146/annurev-arplant-042110-103811.

Hsin, J., Strümpfer, J., Şener, M., Qian, P., Hunter, C.N., Schulten, K., 2010a. Energy transfer dynamics in an RC–LH1–PufX tubular photosynthetic membrane. New J. Phys. 12, (8). https://doi.org/10.1088/1367-2630/12/8/085005 085005.

Hsin, J., Chandler, D.E., Gumbart, J., Harrison, C.B., Sener, M., Strumpfer, J., et al, 2010b. Self-Assembly of Photosynthetic Membranes. ChemPhysChem. 11 (6), 1154–1159. https://doi.org/10.1002/cphc.200900911.

Huo, Y., Shi, Y., Wang, Q., Li, L., Yu, L., Wang, P., et al, 2016. Spectroscopic properties of LH2 from *Thermochromatium tepidum* in liposome and detergent micelles. *Gaodeng Xuexiao Huaxue Xuebao*/. Chem. J. Chin. Univ. 37 (9), 1678–1685. https://doi.org/10.7503/cjcu20160277.

Ikemoto, H., Tubasum, S., Pullerits, T., Ulstrup, J., Chi, Q., 2013. Nanoscale confinement and fluorescence effects of bacterial light harvesting complex LH2 in mesoporous silicas. J. Phys. Chem. C. 117 (6), 2868–2878. https://doi.org/10.1021/jp311239y.

Kiley, P.J., Kaplan, S., 1988. Molecular genetics of photosynthetic membrane biosynthesis in *Rhodobacter sphaeroides*. Microbiol. Rev. 52 (1), 50–69. https://doi.org/10.1128/mr.52.1.50-69.1988.

Kiley, P.J., Varga, A., Kaplan, S., 1988. Physiological and structural analysis of light-harvesting mutants of *Rhodobacter sphaeroides*. J. Bacteriol. 170 (3), 1103–1115. https://doi.org/10.1128/jb.170.3.1103-1115.1988.

Koolhaas, M.H.C., Frese, R.N., Fowler, G.J.S., Bibby, T.S., Georgakopoulou, S., Van der Zwan, G., et al, 1998. Identification of the upper exciton component of the B850 bacteriochlorophylls of the

LH2 antenna complex, using a B800-free mutant of *Rhodobacter sphaeroides*. Biochemistry. 37 (14), 4693–4698. https://doi.org/10.1021/bi973036l.

Kotecha, A., Georgiou, T., Papiz, M.Z., 2013. Evolution of low-light adapted peripheral light-harvesting complexes in strains of *Rhodopseudomonas palustris*. Photosyn. Res. 114 (3), 155–164. https://doi.org/10.1007/s11120-012-9791-0.

Lapouge, K., Näveke, A., Gall, A., Ivancich, A., Seguin, J., Scheer, H., et al, 1999. Conformation of bacteriochlorophyll molecules in photosynthetic proteins from purple bacteria. Biochemistry. 38 (34), 11115–11121. https://doi.org/10.1021/bi990723z.

LaSarre, B., Kysela, D.T., Stein, B.D., Ducret, A., Brun, Y.V., McKinlay, J.B., 2018. Restricted localization of photosynthetic intracytoplasmic membranes (ICMs) in multiple genera of purple nonsulfur bacteria. MBio. 9 (4), e00780–e818. https://doi.org/10.1128/mBio.00780-18.

Li, H., Wang, Y., Ye, M., Li, S., Li, D., Ren, H., et al, 2020. Dynamical and allosteric regulation of photoprotection in light harvesting complex II. Sci. China Chem. 63 (8), 1121–1133. https://doi.org/10.1007/s11426-020-9771-2.

Li, K., Zhao, C., Yue, H., Yang, S., 2014. A unique low light adaptation mechanism in *Rhodobacter azotoformans*. J. Basic Microbiol. 54 (12), 1350–1357. https://doi.org/10.1002/jobm.201400422.

Lommen, M.A.J., Takemoto, J., 1978. Ultrastructure of carotenoid mutant strain R-26 of *Rhodopseudomonas sphaeroides*. Arch. Microbiol. 118 (3), 305–308. https://doi.org/10.1007/BF00429122.

Ma, F., Kimura, Y., Yu, L.J., Wang, P., Ai, X.C., Wang, Z.Y., et al, 2009. Specific Ca^{2+}-binding motif in the LH1 complex from photosynthetic bacterium *Thermochromatium tepidum* as revealed by optical spectroscopy and structural modeling. FEBS J. 276 (6), 1739–1749. https://doi.org/10.1111/j.1742-4658.2009.06905.x.

Mascle-Allemand, C., Lavergne, J., Bernadac, A., Sturgis, J.N., 2008. Organisation and function of the *Phaeospirillum molischianum* photosynthetic apparatus. Biochim. Biophys. Acta - Bioenerg. 1777 (12), 1552–1559. https://doi.org/10.1016/j.bbabio.2008.09.010.

Maudinas, B., Oelze, J., Villoutreix, J., Reisinger, O., 1973. The influence of 2-hydroxybiphenyl on membranes of *Rhodospirillum rubrum*. Archiv. Mikrobiol. 93 (3), 219–228. https://doi.org/10.1007/BF00412021.

Mirkovic, T., Ostroumov, E.E., Anna, J.M., Van Grondelle, R., Scholes, G.D., 2017. Light absorption and energy transfer in the antenna complexes of photosynthetic organisms. Chem. Rev. 117 (2), 249–293. https://doi.org/10.1021/acs.chemrev.6b00002.

Ng, I.W., Adams, P.G., Mothersole, D.J., Vasilev, C., Martin, E.C., Lang, H.P., et al, 2011. Carotenoids are essential for normal levels of dimerisation of the RC–LH1–PufX core complex of *Rhodobacter sphaeroides*: characterisation of R-26 as a crtB (phytoene synthase) mutant. Biochim. Biophys. Acta – Bioenerg. 1807 (9), 1056–1063. https://doi.org/10.1016/j.bbabio.2011.05.020.

Niedzwiedzki, D.M., Hunter, C.N., Blankenship, R.E., 2016. Evaluating the nature of so-called S*-state feature in transient absorption of carotenoids in light-harvesting complex 2 (LH2) from purple photosynthetic bacteria. J. Phys. Chem. B. 120 (43), 11123–11131. https://doi.org/10.1021/acs.jpcb.6b08639.

Ogren, J.I., Tong, A.L., Gordon, S.C., Chenu, A., Lu, Y., Blankenship, R.E., et al, 2018. Impact of the lipid bilayer on energy transfer kinetics in the photosynthetic protein LH2. Chem. Sci. 9 (12), 3095–3104. https://doi.org/10.1039/C7SC04814A.

Pflock, T., Dezi, M., Venturoli, G., Cogdell, R.J., Köhler, J., Oellerich, S., 2008. Comparison of the fluorescence kinetics of detergent-solubilized and membrane-reconstituted LH2 complexes from *Rps. acidophila* and *Rb. sphaeroides*. Photosyn. Res. 95 (2), 291–298. https://doi.org/10.1007/s11120-007-9245-2.

Pribil, M., Labs, M., Leister, D., 2014. Structure and dynamics of thylakoids in land plants. J. Exp. Bot. 65 (8), 1955–1972. https://doi.org/10.1093/jxb/eru090.

Qian, P., Papiz, M.Z., Jackson, P.J., Brindley, A.A., Ng, I.W., Olsen, J.D., et al, 2013. Three-dimensional structure of the *Rhodobacter sphaeroides* RC-LH1-PufX complex: dimerization and quinone channels promoted by PufX. Biochemistry. 52 (43), 7575–7585. https://doi.org/10.1021/bi4011946.

Qian, P., Siebert, C.A., Wang, P., Canniffe, D.P., Hunter, C.N., 2018. Cryo-EM structure of the *Blastochloris viridis* LH1–RC complex at 2.9 Å. Nature. 556 (7700), 203–208. https://doi.org/10.1038/s41586-018-0014-5.

Qian, P., Swainsbury, D.J., Croll, T.I., Salisbury, J.H., Martin, E.C., Jackson, P.J., et al, 2021a. Cryo-EM structure of the monomeric *Rhodobacter sphaeroides* RC–LH1 core complex at 2.5 Å. Biochem. J. 478 (20), 3775–3790. https://doi.org/10.1042/BCJ20210631.

Qian, P., Swainsbury, D.J., Croll, T.I., Castro-Hartmann, P., Divitini, G., Sader, K., et al, 2021b. Cryo-EM structure of the *Rhodobacter sphaeroides* light-harvesting 2 complex at 2.1 Å. Biochemistry 60 (44), 3302–3314. https://doi.org/10.1021/acs.biochem.1c00576.

Rochaix, J.D., 2014. Regulation and dynamics of the light-harvesting system. Annu. Rev. Plant. Biol. 65 (1), 287–309. https://doi.org/10.1146/annurev-arplant-050213-040226.

Saga, Y., Hirota, K., 2016. Determination of the molar extinction coefficients of the B800 and B850 absorption bands in light-harvesting complexes 2 derived from three purple photosynthetic bacteria *Rhodoblastus acidophilus*, *Rhodobacter sphaeroides*, and *Phaeospirillum molischianum* by extraction of bacteriochlorophyll *a*. Anal. Sci. 32 (7), 801–804. https://doi.org/10.2116/analsci.32.801.

Scheuring, S., Sturgis, J.N., 2009. Atomic force microscopy of the bacterial photosynthetic apparatus: plain pictures of an elaborate machinery. Photosyn. Res. 102 (2), 197–211. https://doi.org/10.1007/s11120-009-9413-7.

Seyrig, C., Le Griel, P., Cowieson, N., Perez, J., Baccile, N., 2020a. Synthesis of multilamellar walls vesicles polyelectrolyte-surfactant complexes from pH-stimulated phase transition using microbial biosurfactants. J. Colloid Interface Sci. 580, 493–502. https://doi.org/10.1016/j.jcis.2020.07.021.

Seyrig, C., Kignelman, G., Thielemans, W., Le Griel, P., Cowieson, N., Perez, J., et al, 2020b. Stimuli-Induced Nonequilibrium Phase Transitions in Polyelectrolyte-Surfactant Complex Coacervates. Langmuir. 36 (30), 8839–8857. https://doi.org/10.1021/acs.langmuir.0c01177.

Singharoy, A., Maffeo, C., Delgado-Magnero, K.H., Swainsbury, D. J., Sener, M., Kleinekathöfer, U., et al, 2019. Atoms to phenotypes: molecular design principles of cellular energy metabolism. Cell. 179 (5), 1098–1111. https://doi.org/10.1016/j.cell.2019.10.021.

Sonani, R.R., Gardiner, A., Rastogi, R.P., Cogdell, R., Robert, B., Madamwar, D., 2018. Site, trigger, quenching mechanism and recovery of non-photochemical quenching in cyanobacteria: recent updates. Photosyn. Res. 137 (2), 171–180. https://doi.org/10.1007/s11120-018-0498-8.

Sumino, A., Dewa, T., Noji, T., Nakano, Y., Watanabe, N., Hildner, R., et al, 2013. Influence of phospholipid composition on self-assembly and energy-transfer efficiency in networks of light-harvesting 2 complexes. J. Phys. Chem. B. 117 (36), 10395–10404. https://doi.org/10.1021/jp4047819.

Varga, A.R., Staehelin, L., 1983. Spatial differentiation in photosynthetic and non-photosynthetic membranes of *Rhodopseudomonas palustris*. J. Bacteriol. 154 (3), 1414–1430. https://doi.org/10.1128/jb.154.3.1414-1430.1983.

Xiong, J., Bauer, C.E., 2002. Complex evolution of photosynthesis. Annu. Rev. Plant. Biol. 53 (1), 503–521. https://doi.org/10.1146/annurev.arplant.53.100301.135212.

Yu, J., Fu, L.M., Yu, L.J., Shi, Y., Wang, P., Wang-Otomo, Z.Y., et al, 2017. Carotenoid singlet fission reactions in bacterial light harvesting complexes as revealed by triplet excitation profiles. J. Am. Chem. Soc. 139 (44), 15984–15993. https://doi.org/10.1021/jacs.7b09809.

Yu, L.J., Suga, M., Wang-Otomo, Z.Y., Shen, J.R., 2018. Structure of photosynthetic LH1–RC supercomplex at 1.9 Å resolution. Nature 556 (7700), 209–213. https://doi.org/10.1038/s41586-018-0002-9.